

CrystEngComm

Accepted Manuscript



This is an *Accepted Manuscript*, which has been through the RSC Publishing peer review process and has been accepted for publication.

Accepted Manuscripts are published online shortly after acceptance, which is prior to technical editing, formatting and proof reading. This free service from RSC Publishing allows authors to make their results available to the community, in citable form, before publication of the edited article. This *Accepted Manuscript* will be replaced by the edited and formatted *Advance Article* as soon as this is available.

To cite this manuscript please use its permanent Digital Object Identifier (DOI®), which is identical for all formats of publication.

More information about *Accepted Manuscripts* can be found in the [Information for Authors](#).

Please note that technical editing may introduce minor changes to the text and/or graphics contained in the manuscript submitted by the author(s) which may alter content, and that the standard [Terms & Conditions](#) and the [ethical guidelines](#) that apply to the journal are still applicable. In no event shall the RSC be held responsible for any errors or omissions in these *Accepted Manuscript* manuscripts or any consequences arising from the use of any information contained in them.

Cite this: DOI: 10.1039/c0xx00000x

www.rsc.org/xxxxxx

YOF Nano/micro-crystals: Morphology Controlled Hydrothermal Synthesis and Luminescence Properties

Yang Zhang,^{a,b} Xuejiao Li,^{a,b} Dongling Geng,^{a,b} Mengmeng Shang,^{a,b} Hongzhou Lian,^a Ziyong Cheng,^a and Jun Lin^{a,*}

Received (in XXX, XXX) Xth XXXXXXXXXX 201X, Accepted Xth XXXXXXXXXX 201X

DOI: 10.1039/b000000x

Uniform YOF nano/micro-crystals with nanospheres and micro-rods morphologies have been synthesized by simply modulating the pH values of the initial solution through a facile hydrothermal route without using any morphology controlling agent. The possible formation mechanism of the micro-rods has been proposed on the basis of a series of time-dependent experiments. XRD, FT-IR, TG-DTA, Raman spectra, SEM, TEM, as well as down-conversion (DC) luminescence (photoluminescence, cathodoluminescence) and up-conversion (UC) luminescence spectra are used to characterize the resulting YOF samples. The results of DC and UC luminescence properties prove that the as-synthesized YOF are excellent host lattices for rare earth luminescence. Among the different morphologies, YOF with micro-rods morphology presents the strongest luminescence intensity which may be due to the larger size and the fewer quenching sites, confirmed by the results of morphology-dependent luminescence intensity.

1. Introduction

Recently, rare earth ions (Ln^{3+}) doped nano/micro-luminescent materials have aroused fast growing interest because of their fascinating optical characteristics arising from the intra 4f transitions, such as narrow emission bands, long-lived luminescence, large Stokes or anti-Stokes shifts.¹⁻⁸ Generally, the luminescence types can be categorized as down-conversion (DC) and up-conversion (UC) luminescence. DC is typical Stokes emission process under ultra-violet (UV) or electron beam (high energy) direct excitation, while UC is well known as anti-Stokes emission process under near-infrared (NIR) or infrared light (IR) (low energy) excitation.⁹⁻¹² The former is widely applied in modern lighting and display fields such as white-light emitting diodes (WLEDs), plasma display panels (PDPs), field emission displays (FEDs) and so on.¹³⁻¹⁷ The later is important for applications in areas as diverse as photonics, biomedicine, biological imaging and therapeutics.¹⁸⁻²¹ Hitherto, the use of shape-control agents during the crystallization process is a typical and efficient strategy to control the morphologies and sizes, in which the functional groups of the agents can selectively adsorb on crystal facet and achieve to modulate the kinetics of the crystal growth.²²⁻²⁵ However, the obtained samples always suffer from the unavoidable surface contamination due to the residual organic surfactants, which would affect the physical and chemical properties of the final products.²⁶⁻²⁸ Thus, it is challenging to establish an efficient method to synthesize size and morphology controlled nano/micro-luminescent materials without the use of organic surfactants.²⁹

Lanthanide oxyfluorides have attracted much attention for applications in the down-conversion (DC) and up-conversion

(UC) luminescence due to the high ionicity, low phonon energy, good optical transparency over a wide wavelength range, high chemical and thermal stability.³⁰⁻³³ Till now, YOF nano/micro-crystals with various morphologies have been successfully synthesized by several techniques such as solid state reaction, sol-gel method, molten salt synthesis, thermolysis method and electrospinning process.³⁴⁻³⁹ However, these approaches suffer from drawbacks such as large crystallites, harsh reaction conditions, high environment loads and complicated processes, which severely hamper their potential application.

Herein, we demonstrate a facile hydrothermal method without organic surfactants to prepare YOF nano/micro-crystals with highly uniformity for the first time. Micro-rods and nanospheres could be easily obtained by simply tuning the pH values of the initial solution. The growth mechanism of micro-rods has been proposed on the basis of series time-dependent experiments. Moreover, a systematic study on the morphology-dependent luminescence properties of the photoluminescence (PL), cathodoluminescence (CL) of YOF: $\text{Tm}^{3+}/\text{Tb}^{3+}/\text{Eu}^{3+}$ and up-conversion (UC) luminescence of YOF: Yb^{3+} , $\text{Er}^{3+}/\text{Tm}^{3+}/\text{Ho}^{3+}$ samples have been investigated and discussed.

2. Experimental

2.1 Materials

The starting materials were commercial RE_2O_3 ($\text{Ln} = \text{Y}, \text{Eu}, \text{Tm}, \text{Yb}, \text{Er}$ and Ho) and Tb_4O_7 (99.999 %, Science and Technology Parent Company of Changchun Institute of Applied Chemistry) and other chemicals were purchased from Beijing Chemical Company. All chemicals were analytical grade reagents and used directly without further purification.

2.2 Preparation

RE(NO₃)₃ (0.5 M) stock solutions were obtained by dissolving the corresponding metal oxides in HNO₃ solution at elevated temperature with agitation. In a typical procedure, stoichiometric amounts of Y(NO₃)₃ and KF were added to 40 mL of deionized water. The mixture was stirred for 15 min. Then, certain quantity of NH₃·H₂O was introduced rapidly into the vigorously stirred solution until pH = 9. After additional agitation for 10 min, the as-obtained solution was transferred to a 50 mL autoclave, sealed, and heated at 180 °C for 12 h, then cooled naturally to room temperature. The resulting precipitates were collected by centrifugation, washed three times with ethanol and deionized water and then dried at 85 °C in air for 12 h. The final YOF products were retrieved through a heat treatment of the precursors at 600 °C in air for 3 h with a heating rate of 1 °C/min. Other samples were prepared by a similar procedure, except for different F⁻ sources as well as different pH conditions. The doped YOF samples were prepared by introducing proper amounts of RE(NO₃)₃ instead of Y(NO₃)₃ to the solution as described above.

2.3 Characterization

Power X-ray diffraction (XRD) measurements were performed on a D8 Focus diffractometer at a scanning rate of 10° / min in the 2θ range from 20° to 70°, with graphite monochromatized Cu Kα radiation (λ = 0.15405 nm). Fourier transform infrared spectroscopy (FT-IR) was performed on a Perkin-Elmer 580B IR spectrophotometer using the KBr pellet technique. Thermogravimetric and differential thermal analysis (TG-DTA) data were recorded with Thermal Analysis Instrument (SDT 2960, TA Instruments, New Castle, DE) with the heating rate of 10° / min in an air flow of 100 mL/min. The morphology and composition of the samples were inspected using a field-emission scanning electron microscope (FE-SEM, S-4800, Hitachi) equipped with an energy-dispersive X-ray (EDX) spectrometer. Transmission electron microscopy (TEM) were recorded using a FEI Tecnai G2S-Twin with a field-emission gun operating at 200 kV. Images were acquired digitally on a Gatan multipole CCD camera. PL excitation and emission spectra were recorded with a Hitachi F-7000 spectrophotometer equipped with a 150 W xenon lamp as the excitation source. CL measurements were carried out in an ultrahigh-vacuum chamber (<10⁻⁸ Torr), where the phosphors were excited by an electron beam, and the emission spectra were recorded using an F-7000 spectrophotometer. Raman spectrum was collected using a micro-Raman spectrometer (Renishaw) with a laser of 532 nm wavelength. The luminescence decay curves were obtained from a Lecroy Wave Runner 6100 Digital Oscilloscope (1 GHz) using a tunable laser (pulse width = 4 ns, gate = 50 ns) as the excitation (Continuum Sunlite OPO). Up-conversion (UC) emission spectra were obtained using 980 nm LD Module (K98D08M-30W, China) as the excitation source and detected by R955 (HAMAMATSU) from 400–700 nm. All the measurements were performed at room temperature (RT).

3. Results and discussion

3.1 Phase and Morphology.

Figure 1 shows the XRD patterns of the JCPDS card (no. 71-

2100) for YOF, Y(OH)_{2.02}F_{0.98}, as-prepared precursor sample, YOF annealed at 600 °C and Ln³⁺ doped samples, respectively. The diffraction peaks of the precursor sample basically agree well with the Y(OH)_{2.02}F_{0.98}.

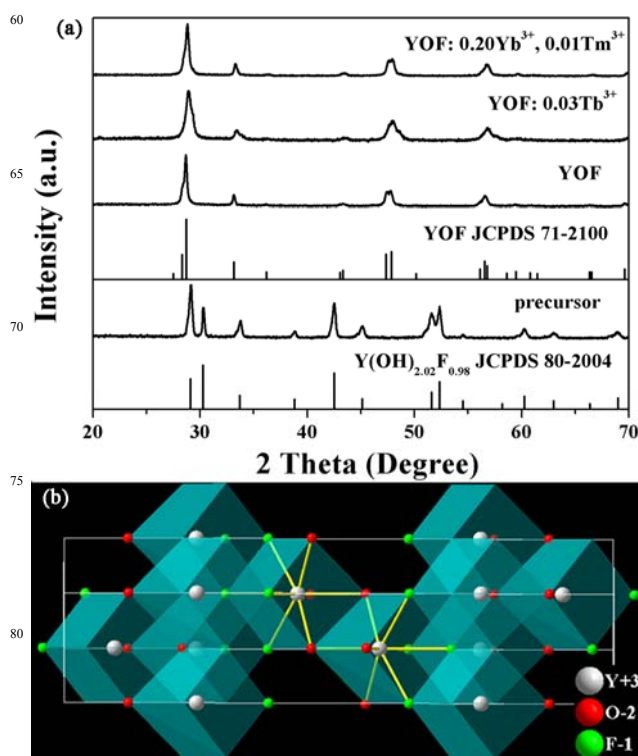


Fig. 1 (a) The XRD patterns of the standard data of YOF (JCPDS No.71-2100), Y(OH)_{2.02}F_{0.98} (JCPDS No.80-2004), as-prepared precursor samples, YOF annealed at 600 °C, Ln³⁺ doped samples. (b) Crystal structure of the rhombohedral phase YOF.

However, after calcinations at 600 °C for 3h, well-defined diffraction peaks appear, which can be assigned exactly to the rhombohedral phase of YOF (R-3m space group, $a = b = 3.79$ Å, $c = 18.89$ Å). The Y³⁺ ions are coordinated by four oxide and four fluoride anions in a bicapped trigonal antiprism arrangement and all ions (F⁻, O²⁻ and Y³⁺) occupy the six-fold 6c Wyckoff positions with the same C_{3v} site symmetry.^{34, 40, 41} Considering the similar valences and ionic radius, the doped Ln³⁺ ions are efficiently dissolved in the YOF host lattice by replacing the Y³⁺, thus, no obvious shifting of peaks or other impurity phase can be detected which confirmed by the XRD results.⁴²

The FT-IR spectroscopy was conducted for both the precursor and YOF, as shown in Figure 2a and 2b. The broad absorption band located at 3424 cm⁻¹ and 1636 cm⁻¹ can be assigned to the O-H vibration of absorbed water on the sample surface.⁴³ The broad peaks at 1360 cm⁻¹ are due to the bending mode of O-H.⁹ The intense and sharp band at 3641 cm⁻¹ and 750 cm⁻¹ are assigned to the stretching and bending vibrations of Y-OH.^{44, 45} After calcinations the precursor at 600 °C for 3 h, two strong absorption band at 505 cm⁻¹ and 450 cm⁻¹ are present, which indicates the well defined crystallization of YOF, as displayed in Figure 2b.^{34, 46} The EDX spectra further confirm the presence of Y, O and F elements of the precursor sample and YOF as shown

in Figure 2c and 2d. After calcinations, the atomic ratio of Y/O/F is determined to be 0.342/0.355/0.303 (Figure 2d), which is much closer to the theoretical YOF atomic ratio (1/1/1). From the DSC-TG curves of the as-prepared precursor sample shown in Figure 3, three stages of weight loss are observed. The first mass loss occurs around 45 to 200 °C, which seems to be the loss of occlusion water.^{33, 47} A great mass loss occurs between

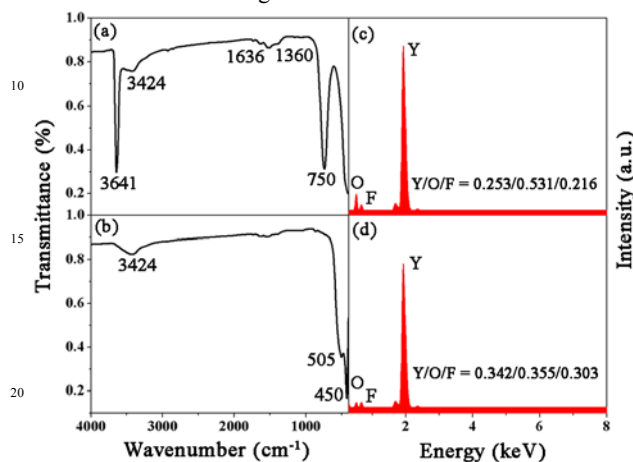


Fig. 2 FT-IR spectra of (a) as-prepared precursor samples and (b) YOF obtained by calcining precursor at 600 °C. EDX spectra of (c) as-prepared precursor samples and (d) YOF obtained by calcining precursor at 600 °C.

250 to 350 °C which is probably attributed to the decomposition of the precursors, and the third one should be caused by the further decomposition of precursors and the formation of YOF at 360-550 °C, basically agreeing well with the above results.³⁸

It should be mentioned that doping of a small amount of other Ln^{3+} in the YOF host does not change the phase, crystallization, and morphology of the YOF products in our present work. So here we only take YOF without doped ions as a typical example to explain the morphologies of the products. It is obvious that the precursor which prepared with KF as F^- source at pH = 9 mainly consists of numerous monodisperse micro-rods with length around 15-20 μm and diameter about 0.5 μm , as the SEM images shown in Figure 4a and 4b. After calcinations at 600 °C for 3 h,

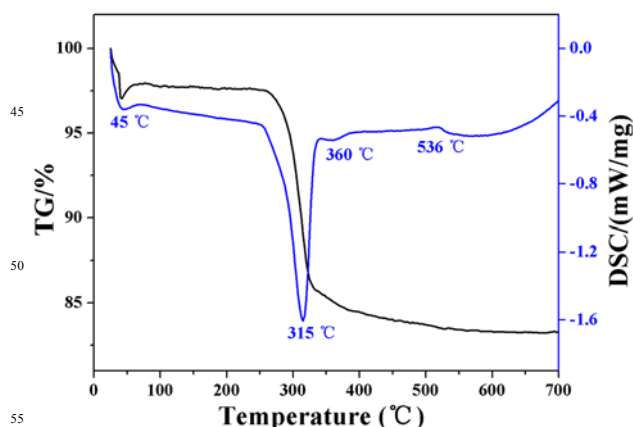


Fig. 3 TG-DSC curves of as-prepared precursor samples with KF at pH = 9.

the size of the micro-rods shrinks and the surface becomes rough along with the splitting at the end due to the decomposition of the precursor and crystallization of YOF, which confirmed by the SEM images of Figure 4c and 4d. In addition, the fine structures of YOF were studied by HRTEM technique, in which the adjacent lattice fringes can be calculated to 0.163 nm, which can be well indexed as d-spacing value of the (116) plane of YOF.

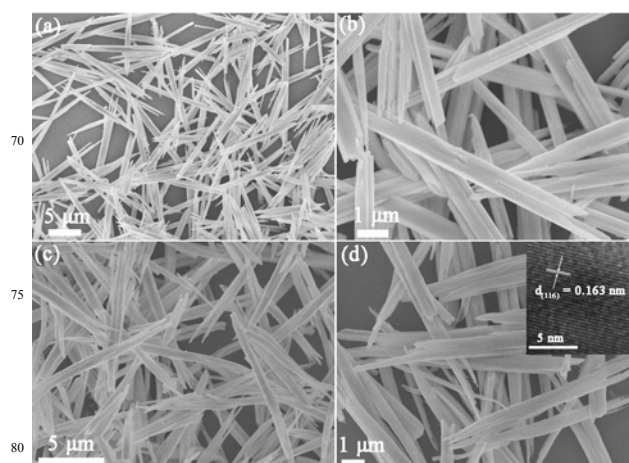


Fig. 4 (a, b) Low and high magnification SEM images of the as-prepared precursor samples and (c, d) Low and high magnification TEM images of the YOF obtained by calcining precursor at 600 °C. Inset of (d) is the corresponding HRTEM images of the YOF samples.

Generally, successful synthesis of nano/micro-materials in a solution-based system not only depends on the intrinsic structure of the target compounds but also requires more fastidious control of the growth parameters such as temperatures, organic additives, types of raw materials, pH values and so forth.^{22, 24, 25, 48-50} The detailed effects of different F⁻ sources and pH values on the morphologies of the final products are shown in the following paragraphs. As displayed in Figure 5a, the crystalline phases of the as-prepared products remain unchanged through the replacement of KF by NH_4F , LiF and NaF. Besides, the morphologies (length and diameter) of the products are a little different from the KF system due to the different attraction and ionicity of K^+ , NH_4^+ , Li^+ and Na^+ , which confirmed by the SEM images shown in Figure 5b-5d.⁵¹ However, things become quite different when we vary the pH values (pH = 11 or 14) of the initial reaction solution with the same F⁻ source (KF). When the pH value was adjusted to 11, the obtained products are composed of nanospheres with diameter about 500 nm (Figure 5e). With further increasing of pH value to 14, the products are mainly composed of well-separated micro-rods with length about 10-15 μm and diameter about 0.5 μm along with nanospheres with diameter about 500 nm, as shown in Figure 5f. From the above results, it seems that pH value plays a critical role in determining the morphologies of the products, which can be explained by the complex interaction and balance between precipitation and the rate of ionic motion. At low pH (pH = 9), the monomer concentration of the solution is still high after nucleation, meanwhile, the rate of the initially formed nuclei motion is high. Thus, it is beneficial for the anisotropic growth of the final product.⁵²⁻⁵⁵

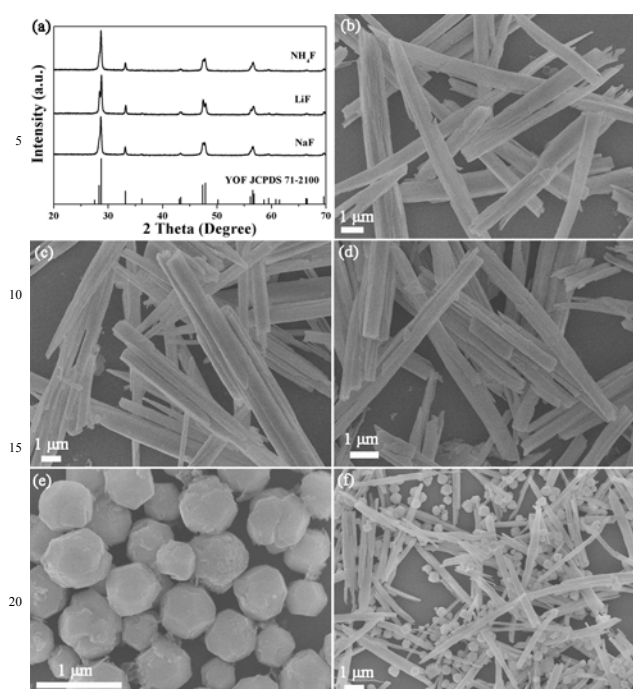


Fig. 5 (a) The XRD patterns of samples prepared with the replacement of KF by $(\text{NH}_4)\text{F}/\text{LiF}/\text{NaF}$. The SEM images of the YOF samples prepared at $\text{pH} = 9$ with different F^- sources, (b) $(\text{NH}_4)\text{F}$, (c) LiF and (d) NaF . The SEM images of YOF prepared with KF at different pH conditions, (e) $\text{pH} = 11$ and (f) $\text{pH} = 14$.

However, the movement of the nuclei is restricted to some extent by increasing the pH value to 11, which results in the formation of isotropic products.^{56, 57} Further increasing the pH value ($\text{pH} = 14$), higher OH^- ion concentration means more nuclei, which may greatly reduce the monomer concentration in solution and reduce the rate of ionic motion. So, the products consist of the mixture of micro-rods and nanospheres. Besides, in hydrothermal synthesis process, the obtained product would take different morphologies so as to decreasing the surface energy in different pH conditions.⁵⁸⁻⁶¹ Thus, choosing an optimal pH value is prerequisite to synthesize YOF with micro-rods ($\text{pH} = 9$) or nanospheres ($\text{pH} = 11$) morphologies.

In order to understand the growing mechanism of the YOF micro-rods, time-dependent experiments have been carried out by keeping other reaction parameters unchanged (KF as F^- source, $\text{pH} = 9$). At the early stage of the hydrothermal reaction for 30 min (Figure 6a), a fast nucleation process occurred and a large numbers of irregular and aggregated nanoparticles were obtained. Prolonging the reaction time to 1 h, some micro-rods with uniform morphology were formed; meanwhile, most of the irregular nanoparticles were consumed, as displayed in Figure 6b. The size of the micro-rods had grown larger in all directions and the uniformity was greatly improved as the reaction continued (3 and 6 h). However, with further increasing the reaction time (12 and 15 h), dissolution and splitting began to appear at the end of the micro-rods (Figure 6e and 6f). On the one hand, the crystal growth rate would increase due to the enhancement of pressure under high temperature in aqueous solution. Kinetically, splitting is related with fast growth rate.⁶²⁻⁶⁴ On the other hand, the

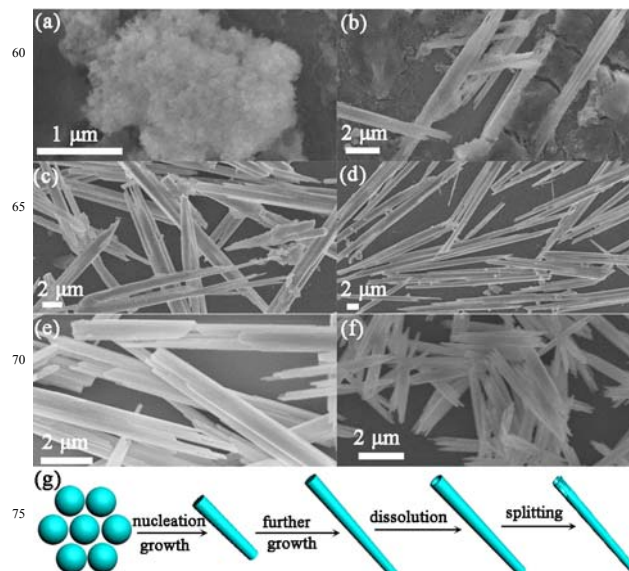
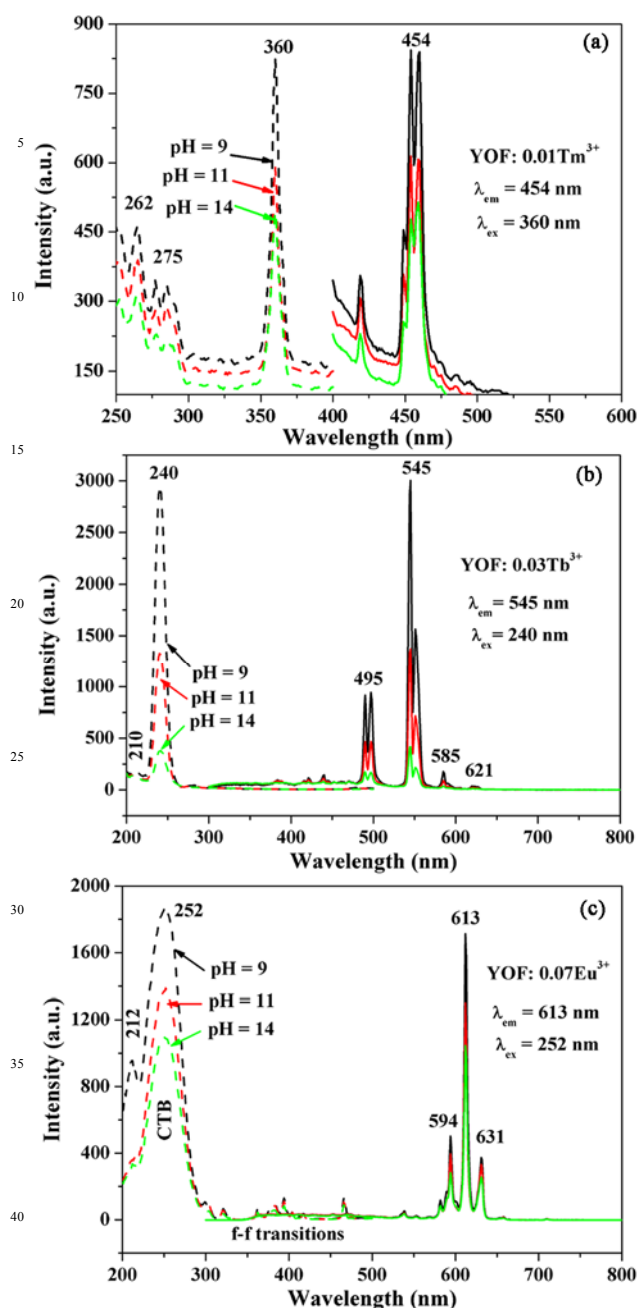


Fig. 6 SEM images of as-prepared precursor samples for different reaction time: (a) 30 min, (b) 1 h, (c) 3 h, (d) 6 h, (e) 12 h and (f) 15 h with KF , $\text{pH} = 9$. (g) Schematic illustration for the formation process of YOF micro-rods.

morphology of the product is associated with the intrinsic nature of lattice symmetry of the hosts. Thermodynamically, the product would take the morphology with lowest energy.^{60, 61, 63, 65} On the basis of the above experimental results and analysis, a schematic illustration for the formation of YOF micro-rods is presented in Figure 6g.

3.2 Down-conversion and Up-conversion Luminescence Properties.

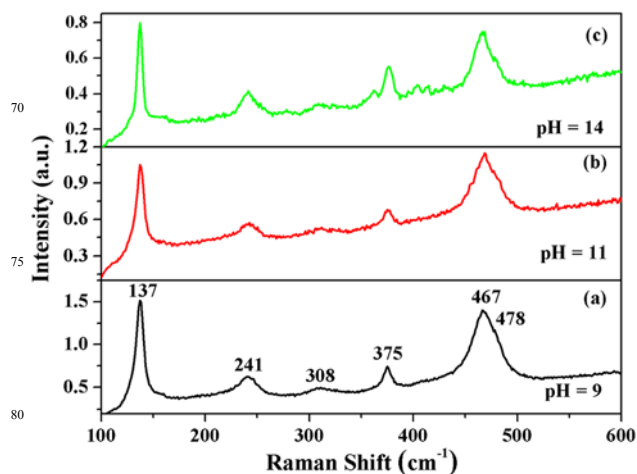
In order to further investigate the dependence of luminescence intensity on the morphologies, the excitation and emission spectra of the as-prepared YOF: Ln^{3+} samples under different pH conditions have been measured as shown in Figure 7. Here it should be mentioned that all the experimental conditions were kept identical in order to avoid the experimental errors. It is obvious that all the three samples share the identical spectral pattern with distinct difference in intensity. As for YOF: 0.01Tm^{3+} (Figure 7a), the excitation spectrum shows sharp peaks at 262, 275 and 360 nm which are ascribed to $^3\text{P}_2 \rightarrow ^3\text{H}_6$, $^3\text{P}_1 \rightarrow ^3\text{H}_6$ and $^1\text{D}_2 \rightarrow ^3\text{H}_6$ transitions of Tm^{3+} ions. The major emission peak of YOF: 0.01Tm^{3+} is at 454 nm corresponding to the transitions $^1\text{D}_2 \rightarrow ^3\text{F}_4$, under excitation with 360 nm irradiation.³³ The excitation spectrum of YOF: 0.03Tb^{3+} shows a strong broad band ($\lambda_{\text{max}} = 240$ nm) with a weak host absorption band at about 210 nm, monitored with the wavelength of 545 nm. Under 240 nm UV radiation excitation, the YOF: 0.03Tb^{3+} gives green emission peaks at 495, 545, 585, and 621 nm, which belongs to the $^5\text{D}_4 \rightarrow ^7\text{F}_J$ ($J = 6, 5, 4, 3$) transitions, respectively.⁶⁶ As displayed in Figure 7c, the excitation spectrum of YOF: 0.07Eu^{3+} shows a strong band with maximum at 252 nm ascribed to the charge transfer transition of $\text{O}^{2-} \rightarrow \text{Eu}^{3+}$, together with a weak host absorption band at about 212 nm and some sharp peaks beyond 300 nm due to $f \rightarrow f$ transitions of Eu^{3+} within its $4f^6$ configuration. Under the excitation of 252 nm, YOF: 0.07Eu^{3+}



45 **Fig. 7** Representative photoluminescence excitation and emission spectra of (a) YOF: 0.01Tm³⁺, (b) YOF: 0.03Tb³⁺ and (c) YOF: 0.07Eu³⁺ with different morphologies.

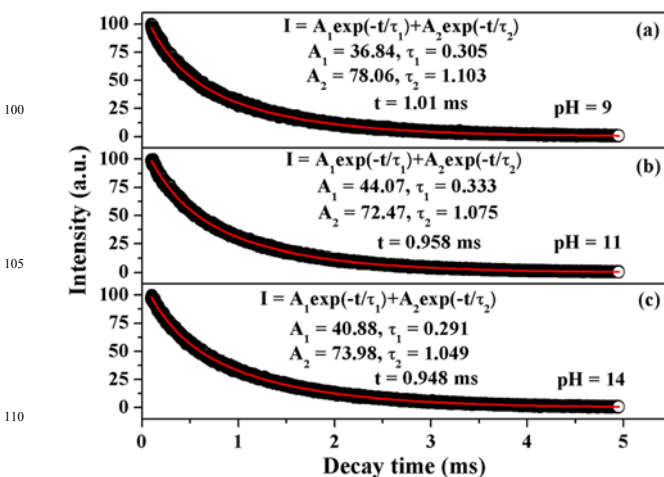
50 samples show linear peaks centered at 594, 613 and 631 nm, which are ascribed to the ⁵D₀ → ⁷F₁ and ⁵D₀ → ⁷F₂ transitions, respectively.^{35,67} Comparing the luminescence intensity of all the samples displayed in Figure 7, it is apparently that the micro-rods samples (pH = 9) show the strongest emission intensity, the nanospheres products (pH = 11) take the second place and the samples prepared at pH = 14 present the weakest emission intensity. Generally, the surface area of the materials increases with a decrease in the size. The larger surface area means a larger number of defects into the phosphor body, which would provide

nonradiative recombination routes for electrons and holes in hosts, thus, decrease the luminescence intensity.^{16, 68} Therefore, the micro-rods samples present the strongest emission intensity. On the other hand, monodisperse spherical structures will lead to high packing densities, low scattering of light, high brightness and high resolution.⁶⁹ As a result, the luminescence intensity of nanospheres sample (pH = 11) is stronger than the mixture of micro-rods and nanospheres (pH = 14).



55 **Fig. 8** Raman spectra of YOF: 0.07Eu³⁺ samples with different morphologies, (a) micro-rods, pH = 9, (b) nanospheres, pH = 11 and (c) mixture micro-rods and nanospheres, pH = 14.

To further reveal the effects of the phonon energies on luminescence intensity of the different morphologies, Raman spectra have been inspected, as shown in Figure 8. It can be seen that the lines at 137 cm⁻¹, 308 cm⁻¹ and 467 cm⁻¹ are due to A_{1g} modes. Meanwhile, the E_g modes are observed at 241 cm⁻¹, 375 cm⁻¹ and 478 cm⁻¹.³⁴ In addition, the comparison of the Raman spectra of the prepared samples also indicates that the phonon modes basically don't change under different pH conditions, however, the intensities vary from each other. Due to the smaller size and larger surface area, the nanospheres possess a poor-order



60 **Fig. 9** Decay curves of the ⁵D₀ → ⁷F₂ emission of Eu³⁺ (λ_{ex} = 252 nm and λ_{em} = 613 nm) in YOF: 0.07Eu³⁺ samples with different morphologies, (a) micro-rods, pH = 9, (b) nanospheres, pH = 11 and (c) mixture micro-rods and nanospheres, pH = 14.

in structure and wider distribution of phonon energies.⁶⁷ In common, smaller size means much more defects, which could affect the distribution of phonon energies and act as quenching sites, leading to nonradiative recombination and luminescence quenching, basically agreeing well with above results.¹⁶

The decay kinetics behavior of different morphologies of YOF: 0.07Eu³⁺ have also been investigated, the corresponding decay curves for the luminescence of the Eu³⁺ ions ($\lambda_{\text{ex}} = 252 \text{ nm}$ and $\lambda_{\text{em}} = 613 \text{ nm}$) are displayed in Figure 9. All the curves can be well fitted into a double exponential function as $I = A_1 \exp(-t/\tau_1) + A_2 \exp(-t/\tau_2)$, and the lifetimes are determined to be 1.01, 0.958, and 0.948 ms for micro-rods, nanospheres and mixture of micro-rods and nanospheres, respectively. The lifetime sequence is consistent with the variation tendency of the luminescence intensity of the three samples, which is attributed to the increase of nonradiative transition rate caused by surface defects.^{70, 71}

The CL properties of as-prepared YOF: Ln³⁺ (Ln = Tm, Tb and Eu) samples have also been investigated in detail considering their potential application in FEDs. Under low-voltage electron beam excitation, the CL spectral profiles of YOF: Ln³⁺ are similar to their PL spectra, which shows the characteristic transitions of

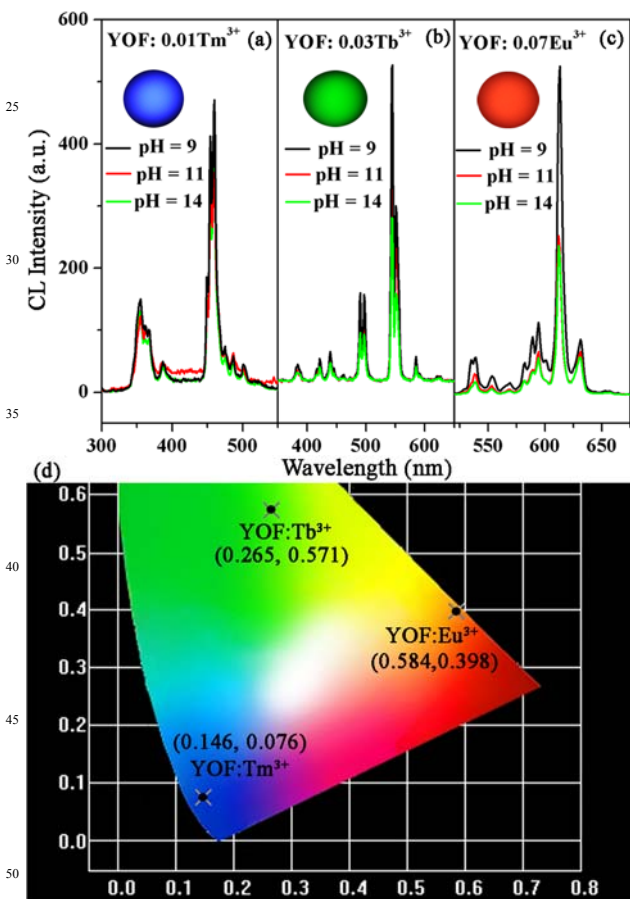


Fig. 10 Typical CL spectra of (a) YOF: 0.01Tm³⁺, (b) YOF: 0.03Tb³⁺ and (c) YOF: 0.07Eu³⁺ with different morphologies, under low-voltage electron beam excitation (accelerating voltage = 3 kV, filament current = 88 mA). The insets are the corresponding CL digital photographs of micro-rods samples. (d) The CIE chromaticity diagram for YOF: 0.01Tm³⁺, YOF: 0.03Tb³⁺ and YOF: 0.07Eu³⁺ with micro-rods morphology.

Ln³⁺ ions and produces bright blue, green and red emissions, respectively, confirmed by the luminescence photographs and CIE coordinates displayed in Figure 10. Also, it is apparently that the samples prepared at pH = 9 present the strongest emission intensity.

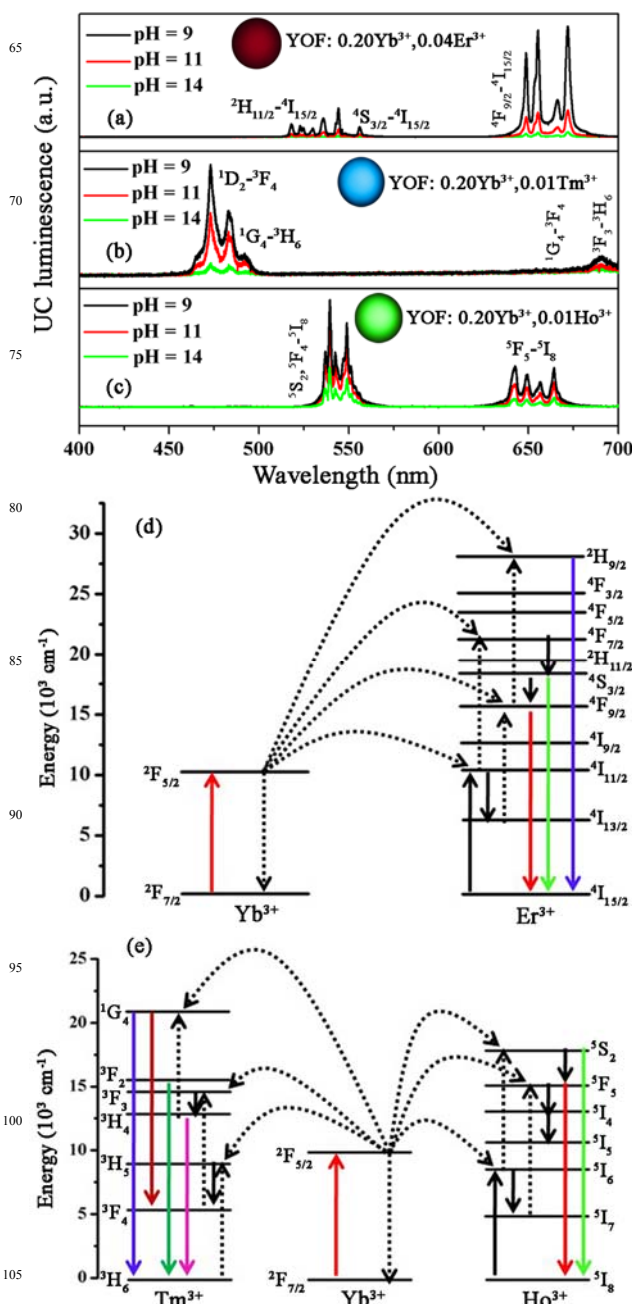


Fig. 11 Typical UC emission spectra of (a) YOF: 0.20Yb³⁺, 0.04Er³⁺, (b) YOF: 0.20Yb³⁺, 0.01Tm³⁺ and (c) YOF: 0.20Yb³⁺, 0.01Ho³⁺ samples with different morphologies under 980 nm laser excitations. The insets are the corresponding UC luminescence digital photographs of micro-rods samples. Schematic illustration of the transition energy levels for the Yb³⁺/Er³⁺ (d) and Yb³⁺/Tm³⁺/Ho³⁺ (e) systems.

Under 980 nm NIR laser excitation, the YOF: Yb³⁺/Er³⁺, YOF: Yb³⁺/Tm³⁺ and YOF: Yb³⁺/Ho³⁺ samples exhibit red, blue and

green emissions respectively, as confirmed by the corresponding luminescent photographs (insets in Figure 11). The UC emission spectrum of YOF: 0.20Yb³⁺, 0.04Er³⁺ is dominated by a strong red emission band at about 670 nm due to ⁴F_{9/2}→⁴I_{15/2} transition with some weak bands in the green emission region with maxima at 530 and 545 nm assigned to the ²H_{11/2}→⁴I_{15/2} and ⁴S_{3/2}→⁴I_{15/2} transitions of the Er³⁺ ions, respectively, as shown in Figure 11a.^{3, 37} The UC luminescence spectrum of YOF: 0.20Yb³⁺, 0.01Tm³⁺ (Figure 11b) consists of two strong blue emission bands centered at 475 and 485 nm, corresponding to the Tm³⁺: ¹G₄→³H₆ and ¹G₄-³H₆ transition, and two weak emission bands at 653 and 693 nm due to ¹G₄→³F₄ and ³F₃→³H₆ transition of Tm³⁺, respectively.^{72, 73} In the case of YOF: 0.20Yb³⁺, 0.01Ho³⁺ in Figure 11c, one green emission band at 540 nm and one red emission band at 650 nm were observed, which were caused by ⁵S₂, ⁵F₄→⁵I₈ and ⁵F₅→⁵I₈ transition of Ho³⁺, respectively.^{9, 74} Figure 11d and 11e show the schematic energy level diagram of Yb³⁺, Er³⁺, Ho³⁺ and Tm³⁺ ions in the YOF: Yb³⁺/Er³⁺/Ho³⁺/Tm³⁺ systems with detailed description of the up-conversion luminescence mechanism.³ The ranking of the UC emission intensities is micro-rods (pH = 9) > nanospheres (pH = 11) > mixture of micro-rods and nanospheres (pH = 14), which is consistent with above discussion.

4. Conclusions

In summary, YOF with various morphologies have been synthesized by a facile hydrothermal route without using any morphology controlling agent. It is observed that pH values play a determining role in modulating the growth process of YOF to govern the formation of final morphology. The growth mechanism of the micro-rods has been proposed on the basis of a series of time-dependent experiments. Under UV light and low-voltage electron beam excitation, YOF: Ln³⁺ (Tm, Tb and Eu) samples show the characteristic f-f transitions of Ln³⁺ ions and give bright blue, green and red emission, respectively. Furthermore, multicolored luminescence could be conferred in a wide triangle region enveloped by three CIE chromaticity coordinate points [YOF: Tm³⁺ (0.146, 0.076), YOF: Tb³⁺ (0.265, 0.571) and YOF: Eu³⁺ (0.584, 0.398)], which is beneficial to enhance display quality. In addition, under 980 nm NIR laser excitation, the Yb³⁺/Er³⁺, Yb³⁺/Tm³⁺ and Yb³⁺/Ho³⁺-co-doped YOF samples exhibit strong red, blue and green UC luminescence, respectively. Morphology-dependent luminescence intensity investigation presents that the emission intensity correlates with the crystallinity and the amounts of surface defects. The DC and UC luminescence results powerfully manifest that the as-prepared YOF are excellent host lattices for obtain efficient luminescence, which may find potential applications in the fields of solid state light, color displays, authentication and security in general, anti-counterfeit and luminescent labels.

Acknowledgements

This project is financially supported by National Basic Research Program of China (Grants 2010CB327704), and the National Natural Science Foundation of China (Grants NSFC 60977013, 51172227, 21221061).

Notes and references

- ^a State Key Laboratory of Rare Earth Resource Utilization, Changchun Institute of Applied Chemistry, Chinese Academy of Sciences, Changchun, 130022, P. R. China. E-mail: jlin@ciac.ac.cn; Fax: +86-431-85698041; Tel: +86-431-85262031
- ^b University of the Chinese Academy of Sciences, Beijing 100049, P. R. China
1. H. A. Höpfe, *Angew. Chem. Int. Ed.*, 2009, **48**, 3572-3582.
2. Y. Liu, D. Tu, H. Zhu and X. Chen, *Chem. Soc. Rev.*, 2013, **42**, 6924-6958.
3. M. Haase and H. Schäfer, *Angew. Chem. Int. Ed.*, 2011, **50**, 5808-5829.
4. F. Wang and X. Liu, *Chem. Soc. Rev.*, 2009, **38**, 976-989.
5. H.-X. Mai, Y.-W. Zhang, R. Si, Z.-G. Yan, L.-d. Sun, L.-P. You and C.-H. Yan, *J. Am. Chem. Soc.*, 2006, **128**, 6426-6436.
6. Z. Tian, H. Liang, B. Han, Q. Su, Y. Tao, G. Zhang and Y. Fu, *J. Phys. Chem. C.*, 2008, **112**, 12524-12529.
7. P. Wang, Y. Wang and L. Tong, *Light Sci Appl*, 2013, **2**, e102.
8. S. Song, Y. Zhang, J. Feng, Y. Xing, Y. Lei, W. Fan and H. Zhang, *Cryst. Growth Des.*, 2008, **9**, 848-852.
9. G. Li, C. Li, Z. Xu, Z. Cheng and J. Lin, *CrystEngComm*, 2010, **12**, 4208-4216.
10. F. Auzel, *Chem. Rev.*, 2004, **104**, 139-174.
11. S. Ye, F. Xiao, Y. X. Pan, Y. Y. Ma and Q. Y. Zhang, *Mater. Sci. Eng., R.*, 2010, **71**, 1-34.
12. S. Song, Y. Zhang, J. Feng, X. Ge, D. Liu, W. Fan, Y. Lei, Y. Xing and H. Zhang, *CrystEngComm*, 2009, **11**, 1987-1993.
13. W.-T. Chen, H.-S. Sheu, R.-S. Liu and J. P. Attfield, *J. Am. Chem. Soc.*, 2012, **134**, 8022-8025.
14. R. J. Xie, N. Hirotsaki, K. Sakuma, Y. Yamamoto and M. Mitomo, *Appl. Phys. Lett.*, 2004, **84**, 5404-5406.
15. C. Liu, S. Zhang, Z. Liu, H. Liang, S. Sun and Y. Tao, *J. Mater. Chem. C*, 2013, **1**, 1305-1308.
16. G. Li, Z. Hou, C. Peng, W. Wang, Z. Cheng, C. Li, H. Lian and J. Lin, *Adv. Funct. Mater.*, 2010, **20**, 3446-3456.
17. C.-H. Huang, T.-W. Kuo and T.-M. Chen, *Acs Appl. Mater. Interfaces.*, 2010, **2**, 1395-1399.
18. W. Feng, C. Han and F. Li, *Adv. Mater.*, 2013, **25**, 5287-5303.
19. P. Li, Q. Peng and Y. Li, *Adv. Mater.*, 2009, **21**, 1945-1948.
20. J. Liu, W. Bu, L. Pan and J. Shi, *Angew. Chem. Int. Ed.*, 2013, **52**, 4375-4379.
21. L. Cheng, C. Wang, X. Ma, Q. Wang, Y. Cheng, H. Wang, Y. Li and Z. Liu, *Adv. Funct. Mater.*, 2013, **23**, 272-280.
22. S. Huang, J. Xu, Z. Zhang, X. Zhang, L. Wang, S. Gai, F. He, N. Niu, M. Zhang and P. Yang, *J. Mater. Chem.*, 2012, **22**, 16136-16144.
23. C. Li, J. Yang, P. Yang, H. Lian and J. Lin, *Chem. Mater.*, 2008, **20**, 4317-4326.
24. X. Wang, J. Zhuang, Q. Peng and Y. Li, *Nature*, 2005, **437**, 121-124.
25. Y. Yin and A. P. Alivisatos, *Nature*, 2004, **437**, 664-670.
26. C.-C. Yang, Y.-H. Yu, B. van der Linden, J. C. Wu and G. Mul, *J. Am. Chem. Soc.*, 2010, **132**, 8398-8406.
27. X. Chen, H. Xu, N. Xu, F. Zhao, W. Lin, G. Lin, Y. Fu, Z. Huang, H. Wang and M. Wu, *Inorg. Chem.*, 2003, **42**, 3100-3106.
28. S. Mourdikoudis and L. M. Liz-Marzán, *Chem. Mater.*, 2013, **25**, 1465-1476.
29. A. M. Kaczmarek and R. Van Deun, *Chem. Soc. Rev.*, 2013, **42**, 8835-8848.
30. K. Zheng, Y. Liu, Z. Liu, Z. Chen and W. Qin, *Dalton Trans.*, 2013, **42**, 5159-5166.
31. Y.-P. Du, Y.-W. Zhang, Z.-G. Yan, L.-D. Sun and C.-H. Yan, *J. Am. Chem. Soc.*, 2009, **131**, 16364-16365.
32. X. Sun, Y. W. Zhang, Y. P. Du, Z. G. Yan, R. Si, L. P. You and C. H. Yan, *Chem. Eur. J.*, 2006, **13**, 2320-2332.
33. Y. Zhang, X. Kang, D. Geng, M. Shang, Y. Wu, X. Li, H. Lian, Z. Cheng and J. Lin, *Dalton Trans.*, 2013, **42**, 14140-14148.
34. J. Hölsä, B. Piriou and M. Räsänen, *Spectrochim. Acta Part A*, 1993, **49**, 465-470.
35. T. Grzyb, M. Węclawiak, T. Pędziński and S. Lis, *Opt. Mater.*, 2013, **35**, 2226-2233.

36. M. Ding, C. Lu, L. Cao, Y. Ni and Z. Xu, *Opt. Mater.*, 2013, **35**, 1283-1287.
37. G. Yi, Y. Peng and Z. Gao, *Chem. Mater.*, 2011, **23**, 2729-2734.
38. R. Yang, G. Qin, D. Zhao, K. Zheng and W. Qin, *J. Fluor. Chem.* 2012, **140**, 38-42.
39. Y. Zhang, D. Geng, X. Kang, M. Shang, Y. Wu, X. Li, H. Lian, Z. Cheng and J. Lin, *Inorganic Chemistry*, 2013, **52**, 12986-12994.
40. J. Hölsä and E. Kestilä, *Journal of the Chemical Society, Faraday Trans.*, 1995, **91**, 1503-1509.
41. T. Grzyb, M. Węclawiak and S. Lis, *J. Alloys Compd.*, 2012, **539**, 82-89.
42. R. D. Shannon, *Acta Crystallogr. Sec. A*, 1976, **32**, 751-767.
43. H. Zhu, D. Yang, H. Yang, L. Zhu, D. Li, D. Jin and K. Yao, *J. Nanopart. Res.*, 2008, **10**, 307-312.
44. M. Aghazadeh, A. Nozad, H. Adelkhani and M. Ghaemi, *J. Electrochem. Soc.*, 2010, **157**, D519-D522.
45. T. Yousefi and M. Aghazadeh, *J. Nanoeng. Nanomanuf.*, 2012, **2**, 248-252.
46. J. Hölsä, E. Säilynoja, H. Rahiala and J. Valkonen, *Polyhedron*, 1997, **16**, 3421-3427.
47. X. Zhang, P. Yang, D. Wang, J. Xu, C. Li, S. Gai and J. Lin, *Cryst. Growth Des.*, 2011, **12**, 306-312.
48. Q. Zhang, S.-J. Liu and S.-H. Yu, *J. Mater. Chem.*, 2009, **19**, 191-207.
49. H. C. Zeng, *J. Mater. Chem.*, 2011, **21**, 7511-7526.
50. S.-N. Zhao, S.-Q. Su, X.-Z. Song, M. Zhu, Z.-M. Hao, X. Meng, S.-Y. Song and H.-J. Zhang, *Cryst. Growth Des.*, 2013, **13**, 2756-2765.
51. M. Wang, Q.-L. Huang, J.-M. Hong, X.-T. Chen and Z.-L. Xue, *Cryst. Growth Des.*, 2006, **6**, 2169-2173.
52. X. Wang, X. M. Sun, D. Yu, B. S. Zou and Y. Li, *Adv. Mater.*, 2003, **15**, 1442-1445.
53. Y. Xia, P. Yang, Y. Sun, Y. Wu, B. Mayers, B. Gates, Y. Yin, F. Kim and H. Yan, *Adv. Mater.*, 2003, **15**, 353-389.
54. Z. A. Peng and X. Peng, *J. Am. Chem. Soc.*, 2001, **123**, 183-184.
55. M. Zhao, L. Li, J. Zheng, L. Yang and G. Li, *Inorg. Chem.*, 2013, **52**, 807-815.
56. X. Wang and Y. Li, *Angew. Chem. Int. Ed.*, 2002, **41**, 4790-4793.
57. C. Li, J. Yang, Z. Quan, P. Yang, D. Kong and J. Lin, *Chem. Mater.*, 2007, **19**, 4933-4942.
58. M. Zhao, G. Li, L. Li, L. Yang and J. Zheng, *Cryst. Growth Des.*, 2012, **12**, 3983-3991.
59. M. Zhao, G. Li, J. Zheng, L. Li, H. Wang and L. Yang, *CrystEngComm*, 2011, **13**, 6251-6257.
60. H. Lin, L. Li, M. Zhao, X. Huang, X. Chen, G. Li and R. Yu, *J. Am. Chem. Soc.*, 2012, **134**, 8328-8331.
61. M. Zhao, L. Li, H. Lin, L. Yang and G. Li, *Chem. Commun.*, 2013, **49**, 7046-7048.
62. R. L. Penn and J. F. Banfield, *Geochim. Cosmochim. Ac.*, 1999, **63**, 1549-1557.
63. J. Tang and A. P. Alivisatos, *Nano Letters*, 2006, **6**, 2701-2706.
64. S. Song, Y. Zhang, Y. Xing, C. Wang, J. Feng, W. Shi, G. Zheng and H. Zhang, *Adv. Funct. Mater.*, 2008, **18**, 2328-2334.
65. H. Deng, C. Liu, S. Yang, S. Xiao, Z.-K. Zhou and Q.-Q. Wang, *Cryst. Growth Des.*, 2008, **8**, 4432-4439.
66. L. Yu, H. Song, Z. Liu, L. Yang and S. L. Z. Zheng, *J. Phys. Chem. B*, 2005, **109**, 11450-11455.
67. A. Feinle, F. Lavoie-Cardinal, J. Akbarzadeh, H. Peterlik, M. Adlung, C. Wickleder and N. Hüsing, *Chem. Mater.*, 2012, **24**, 3674-3683.
68. B. Shao, Q. Zhao, N. Guo, Y. Jia, W. Lv, M. Jiao, W. Lü and H. You, *CrystEngComm*, 2013, **15**, 5776-5783.
69. J. G. Li, X. Li, X. Sun and T. Ishigaki, *J. Phys. Chem. C.*, 2008, **112**, 11707-11716.
70. J. Yang, C. Li, Z. Quan, C. Zhang, P. Yang, Y. Li, C. Yu and J. Lin, *J. Phys. Chem. C.*, 2008, **112**, 12777-12785.
71. M. Zhao, G. Li, J. Zheng, L. Li and L. Yang, *CrystEngComm*, 2012, **14**, 2062-2070.
72. S. Zeng, J. Xiao, Q. Yang and J. Hao, *J. Mater. Chem.* 2012, **22**, 9870-9874.
73. J. H. Chung, J. H. Ryu, S. W. Mhin, K. M. Kim and K. B. Shim, *J. Mater. Chem.* 2012, **22**, 3997-4002.
74. J. Pichaandi, F. C. van Veggel and M. Raudsepp, *Acs Appl. Mater. Interfaces.*, 2009, **2**, 157-164.

75

TOC

The SEM images and multicolored down-conversion and up-conversion luminescence photographs of YOF: Ln³⁺ nano/micro-structures.

5
10
15
20
25
30
35
40
45
50

